BMC Urology

RESEARCH

Open Access

Development and validation of a framework for registration of whole-mount radical prostatectomy histopathology with three-dimensional transrectal ultrasound

Auke Jager[1,2*†], Marije J. Zwart[3,4†], Arnoud W. Postema[5], Daniel L. van den Kroonenberg[1], Wim Zwart[4], Harrie P. Beerlage[1], J. R. Oddens[1,3] and Massimo Mischi[3]

Abstract

Purpose Artificial intelligence (AI) has the potential to improve diagnostic imaging on multiple levels. To develop and validate these AI-assisted modalities a reliable dataset is of utmost importance. The registration of imaging to pathology is an essential step in creating such a dataset. This study presents a comprehensive framework for the registration of 3D transrectal ultrasound (TRUS) to radical prostatectomy specimen (RPS) pathology.

Methods The study enrolled patients who underwent 3D TRUS and were scheduled for radical prostatectomy. A four-step process for registering RPS to TRUS was used: image segmentation, 3D reconstruction of RPS pathology, registration and ground truth calculation. Accuracy was assessed using a target-registration error (TRE) based on landmarks visible on both TRUS and pathology.

Results 20 Sets of 3D TRUS and RPS pathology were included for analyses. The mean TRE was 3.5 mm, (range: 0.4 to 5.4 mm), with TRE values in the apex-base, left-right and posterior-anterior directions of 2.5 mm, 1.1 mm, and 1.4 mm, respectively.

Conclusion The framework proposed in this study accomplishes precise registration between prostate pathology and imaging. The methodologies employed hold the potential for broader application across diverse imaging modalities and other target organs. However, limitations such a small sample size and the need for manual segmentation should be considered when interpreting te results. Future efforts should focus on automating key steps to enhance reproducibility and scalability.

†Auke Jager and Marije J. Zwart contributed equally to this work.

*Correspondence:
Auke Jager
a.jager1@amsterdamumc.nl
[1]Department of Urology, Amsterdam UMC location Vrije Universiteit Amsterdam, De Boelelaan 1117, Amsterdam, the Netherlands
[2]Department of Urology, Amsterdam UMC, University of Amsterdam, Meibergdreef 9, Amsterdam, The Netherlands
[3]Department of Electrical Engineering, Eindhoven University of Technology, Eindhoven, The Netherlands
[4]Angiogenesis Analytics, JADS Venture Campus, 's-Hertogenbosch, AA, The Netherlands
[5]Department of Urology, Leiden University Medical Center, Leiden, the Netherlands

Introduction

Imaging plays an increasingly important role in prostate cancer (PCa) diagnostics. Prostate magnetic resonance imaging (MRI) prior to prostate biopsy is currently the standard of care for patients with a clinical suspicion for PCa [1]. While MRI has greatly improved the diagnostic pathway for PCa, it still has certain limitations related to diagnostic accuracy, availability, cost, and interobserver agreement [2, 3].

As a result, various methods to improve prostate imaging are being investigated. These methods are related to advancements in MRI performance and efficiency, as well as the exploration of alternative imaging modalities such as transrectal ultrasound (TRUS) and prostate-specific membrane antigen (PSMA) positron emission tomography (PET)-based modalities [4–6]. An area of particular interest is the integration of artificial intelligence (AI) into the diagnostic process, which shows potential in improving diagnostic accuracy, reducing interobserver variability, and addressing time-intensity concerns [7–9].

Regarding TRUS as an alternative modality, the multiparametric approach shows promise. This approach combines information from different ultrasound modalities, including Brightness-mode (B-mode), contrast-enhanced ultrasound (CEUS), and shear wave elastography (SWE). Machine learning (ML) techniques have emerged as a valuable tool for integrating and extracting information from these ultrasound modalities [5, 8, 10].

In recent developments, the availability of 3D TRUS has provided further support to these advancements. The capability of imaging the entire prostate gland in a single scan offers evident advantages for the clinical workflow [11–13]. (3D) TRUS-based imaging may be advantageous over MRI due to its cost-effectiveness and wider availability, although its value in clinical practice for PCa diagnosis is not yet established [5].

Ongoing research aims to develop AI methods to detect PCa on different imaging modalities [11]. For development and validation of such methods, a reliable ground truth is required [14]. The best way to obtain this ground truth is through correlation of pre-surgical in-vivo imaging with pathology slides obtained from radical prostatectomy specimens (RPS) [15]. The pathology slides contain information on the localization and characterization of cancerous tissue, which can then be mapped onto the corresponding images recorded in-vivo. However, correlation of pathology to imaging (i.e., registration) poses several challenges.

Following surgery, the RPS is fixated in formalin and sliced into slices of approximately equal size, which are then used to create pathology slides for evaluation by a pathologist. Due to variation in slice thickness, differences between pathology and imaging slice orientation, and RPS deformation, pathology and imaging slices cannot simply be overlaid for correlation [16]. For MRI, multiple registration approaches using open-source ML algorithms have been proposed that reach fairly high levels of accuracy [15, 17]. These approaches cannot be applied to TRUS due to a different slice orientation and prostate deformation due to the pressure applied by the ultrasound probe on the prostate [16].

Previous work has shown promising results using affine and elastic, surface-based registration for in-vivo registration of 2D TRUS with RPS pathology, with a mean target registration error (TRE) of 2.1 mm [18]. However, the validation was limited to a small cohort of seven patients. In contrast, the current study employs a larger dataset and uses 3D TRUS, providing a more robust validation. This paper presents a new framework for the registration of 3D TRUS with 3D RPS pathology and reports on its in-vivo validation. Although the framework is primarily developed for TRUS, it proposes several innovative techniques that can potentially facilitate accurate registration of pathology across different imaging modalities.

Methods

The cohort consisted of patients planned for radical prostatectomy (RP) because of biopsy-proven PCa, prospectively included in a multicentre study. The trial protocol for this study has been published [11]. The framework for TRUS-pathology registration can be separated in four steps (1) TRUS acquisition and segmentation (2) RPS pathology handling and 3D reconstruction, (3) TRUS-pathology registration and (4) calculation of ground truth. A summary of the data acquisition and handling process is visually represented in Fig. 1.

Three-dimensional transrectal prostate ultrasound acquisition and segmentation

The ultrasound acquisition protocol has been previously described in detail in the published trial protocol paper [11]. In brief, all examinations were performed using a LOGIQ™ E10 ultrasound system equipped with an RIC 5-9D 3D endocavitary probe (GE Healthcare, Chicago, IL, USA). Automatic 120° volumetric sweeps captured B-mode, shear-wave elastography, and contrast-enhanced images (Fig. 2). A custom fixture secured the probe to ensure stable acquisition (Fig. 3).

Acquisition settings were standardized to ensure consistency and reproducibility across all imaging modalities.

B-mode Gain was set at 55 dB with a dynamic range of 69 dB. Depth was adjusted according to prostate size. The transducer frequency was 9 MHz, with a mechanical index (MI) of 1.30 and power level at 100%.

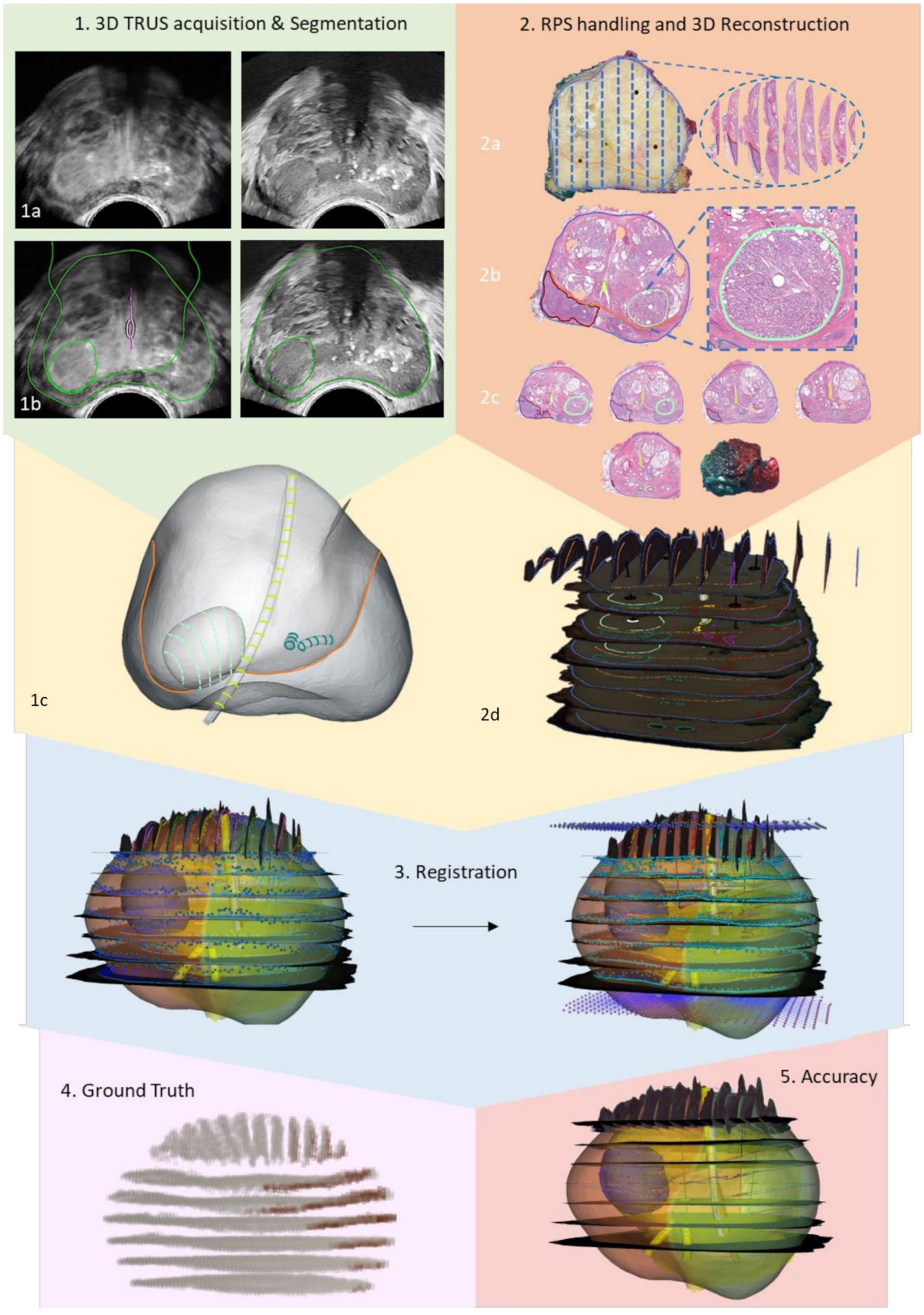

Fig. 1 (See legend on next page.)

(See figure on previous page.)

Fig. 1 Summary of data acquisition, registration process and accuracy calculation. (1) Ultrasound Imaging: Transversal views of CEUS and B-mode scans are shown without segmentation (**1a**) and with segmentation of anatomical structures (**1b**). (**1c**) displays the 3D prostate model generated from ultrasound-based segmentation. (2) Pathology Slides: Pathology data includes the parasagitally divided apical slice (**2a**) and whole-mount slides spanning from apex to base (**2b** and **2c**). (**2d**) demonstrates the 3D prostate reconstruction derived from the pathology slides. Note the clearly discernable landmark (BPH nodule) visible in both the TRUS scan and the pathology images (**1b** and **2b**). (3) Registration: The registration process is illustrated with blue tension lines representing alignment losses. (4) Ground Truth: Sparse, binary ground truth data is presented, where white indicates benign tissue and orange indicates malignant tissue. (5) Accuracy Calculation: The accuracy of the process is calculated and summarized. BPH = Benign Prostate Hyperplasia, CEUS = Contrast-Enhanced Ultrasound, RPS = Radical Prostatectomy Specimen, TRUS = Transrectal Ultrasound

CEUS Gain was set at 55 dB with a dynamic range of 42 dB. Depth was adjusted according to prostate size. The transducer frequency was 3.5 MHz, with an MI of 0.10 and a power level of 10%. At the start of the acquisition, a standardized bolus of 2.4 mL of contrast agent (SonoVue; Bracco, Geneva, Switzerland) was administered intravenously, followed by a 10 mL saline flush. The volume frame rate was set at 1 volume per second to capture dynamic contrast perfusion. The total CEUS acquisition time was 2 min.

The 3D SWE mode is performed using a pre-programmed macro feature on the ultrasound machine, capturing 25 SWE images at 5° intervals across a 120° sweep from the basal to the apical side of the prostate. Imaging parameters were set to optimize signal quality, with a gain of 15 dB, a dynamic range of 20 dB, a power level of 100%, and MI of 1.4. The transducer operated at a frequency of 9 MHz.

Further details on the acquisition protocol are provided in the published trial protocol paper [11].

Image processing consisted of manual segmentation of anatomical structures, using a segmentation tool developed specifically for this study by Angiogenesis Analytics (AA, 's-Hertogenbosch, the Netherlands). Segmentations were performed by AJ or AP, with respectively 4 and 8 years of experience with TRUS. Standard segmentation consisted of the prostate border, the border between peripheral zone (PZ) and transitional zone (TZ), and the urethra. Additional segmentation of other anatomical structures (utriculus and ejaculatory ducts) and landmarks (e.g., calcifications and cysts) were only performed when clearly visible on both ultrasound and pathology.

Radical prostatectomy pathology

Radical prostatectomy specimen handling

RPS handling was performed according to a study specific protocol [11]. To facilitate accurate 3D pathology reconstruction and subsequent registration to TRUS, certain steps were included in the protocol. Prior to fixation in formalin, four intravenous cannulas were inserted in four different quadrants of the RPS from apex to base. After at least 24 h of fixation in formalin, the cannulas were removed, the RPS was cut into 4-mm thick slices from apex to base using the TruSlice specimen cut up system (CellPath ltd, Newtown, UK) and a photo of the gross pathology slices was captured. The most apical and basal slice were further divided parasagittally in 4-mm strips. Pathology slides were cut at 4-µm thickness from the gross pathology slices using a microtome and scanned on high resolution (40x enlargement, 20x objective, 2.1 camera lens) with a Pannoramic 1000 Digital Slide Scanner (3DHISTECH, H-1141 Budapest, Hungary). Digital pathology slices were annotated according to study protocol by a pathologist using a web-based pathology annotation tool (Slidescore, Amsterdam, the Netherlands) [11, 19]. Apart from cancerous areas, the annotation protocol also included the same anatomical structures and landmarks segmented on TRUS.

Three-dimensional pathology reconstruction

After annotation, pathology slides were overlaid on the gross image of prostate slices. The gross prostate slices with overlay were then stacked to create a 3D pathology model. The needle holes resulting from the intravenous cannulas were used to prevent rotational and translational errors between the slices. Shrinkage of histopathology slides could be compensated for up to 10%. The apical pathology slices were sequenced from left to right, checked for anterior and posterior orientation, and fitted on the most apical gross prostate slice. The parasagittal pathology slides from the most basal (or bladder neck) slice were not included in the reconstruction.

Registration of pathology to ultrasound images

The registration is defined by both a rigid and a non-rigid transform. By applying first, the rigid, and then the non-rigid transform, the pathology slides are mapped onto the TRUS images, minimising the distance between the visible anatomical structures in both domains. The registration procedure compensates for in-vivo deformation of the prostate caused by pressure from the ultrasound probe, as well as ex-vivo deformation resulting from the excision of the prostate and subsequent fixation in formalin [20]. The full registration algorithm was implemented and visualised in a registration tool (developed by AA), with the individual steps indicated in Fig. 4.

Compensation for probe deformation

During TRUS acquisition, the prostate is deformed in-vivo due to pressure applied by the probe. As this is not present in the pathology slices, compensation of this deformation is required for accurate registration. This is

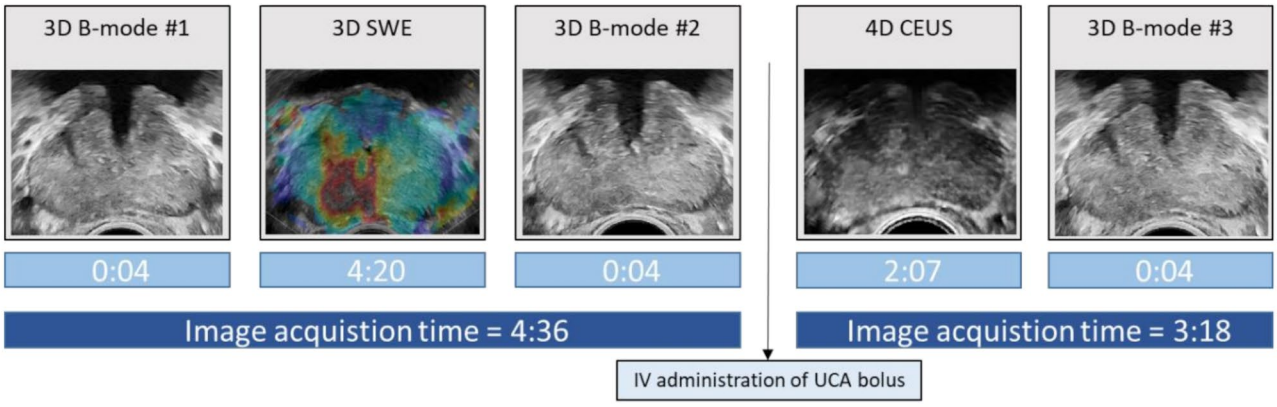

Fig. 2 Image acquisition sequence including acquisition time per ultrasound modality. Note that three separate 3D B-mode acquisitions are performed. These can be used for motion detection and compensation. B-mode = Brightness-mode, CEUS = Contrast Enhanced Ultrasound, SWE = Shear Wave Elastography, IV = Intravenous, UCA = Ultrasound Contrast Agent

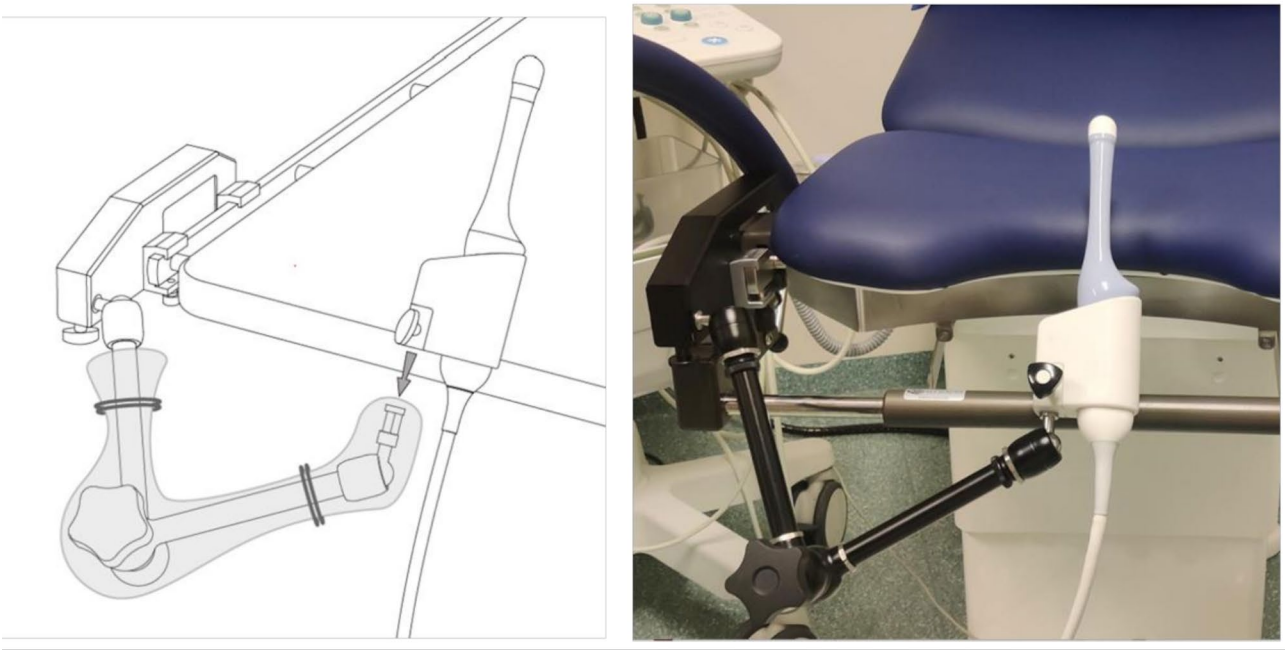

Fig. 3 probe fixture. The probe fixture is attached to the DIN-rail and is used to fix the ultrasound probe in a position to ensure optimal and stable image acquisition

done by modelling the deformation effect of the probe on homogeneous tissue based on a 3D scan of the probe. The inverse of this deformation is then applied to the 3D ultrasound segmentations.

Rigid registration

The rigid registration process aligns the reconstructed prostate pathology with the ultrasound scan domain using translation, rotation, and scaling factors. Translation and rotation parameters position the prostate in the correct spatial orientation, while scaling factors adjust for slice thickness variations and tissue shrinkage during fixation.

Initially, the centers of the prostate boundaries in the ultrasound and pathology domains are aligned along the left-right, anterior-posterior, and apex-base axes. The alignment is refined using an iterative closest point (ICP) algorithm, which pairs anatomical points in the pathology domain with their nearest counterparts in the ultrasound domain. The algorithm minimizes discrepancies between these paired points by calculating a total loss (cost function), defined as the weighted root mean square error (RMSE) of distances across all structures.

To address uncertainties in the apex-base axis due to the exclusion of basal pathology slides, an additional loss term accounts for differences between the desired and

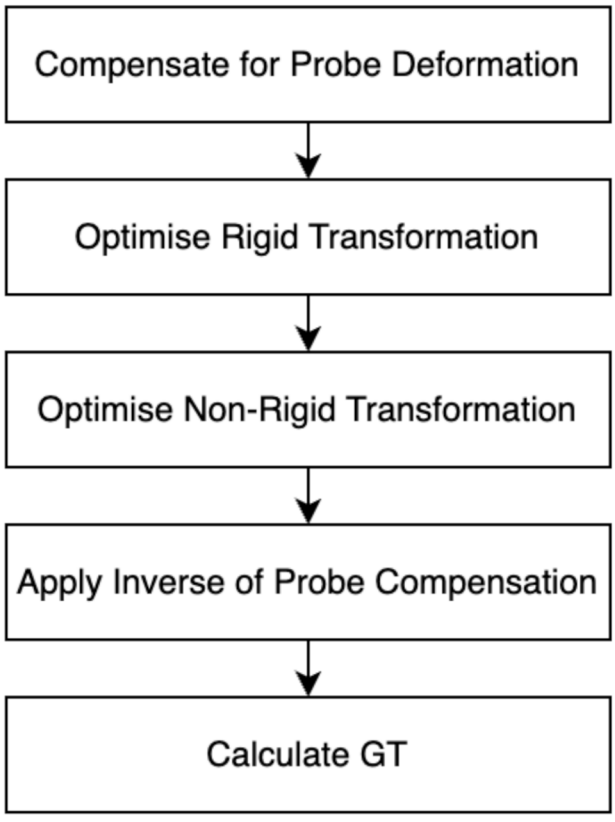

Fig. 4 Registration flowchart. GT = Ground truth

actual base heights. Operators can manually fine-tune parameters such as loss weights, base height, and slice shear to optimize alignment. The blue 'tension' lines in the registration section of Fig. 1 present a visual representation of the point-pairs. Visual inspection of these "tension lines" helps ensure consistency, with adjustments reviewed by a second operator to reach consensus. The process concludes when the loss values stabilize, and no further improvements are identified.

Non-Rigid registration

Non-rigid registration refines alignment by compensating for local tissue deformations after rigid registration. Using the Finite Element Method (FEM), the scan space is divided into a 2 mm grid, and deformation of the grid is applied to optimize the registration by minimizing the RMSE loss between paired points. Modeling tissue elasticity, this step also enforces minimal deformation.

The optimization process iteratively improves the registration for minimal deformation until either the improvement between iterations becomes negligible or a set maximum number of iterations is reached. This step is fully automated and does not require operator input.

Calculation of ground truth

Applying both the rigid and non-rigid transforms, the pathology annotations are mapped onto the 3D ultrasound scan space which was compensated for probe deformation. Therefore, the last step consists of applying the probe deformation to the annotations. Voxels lying inside the registered slides can now be assigned as either malignant or benign, based on the pathology annotations. Note that this does not provide any information on the voxels lying in between the pathology slides. Interpolation techniques are applied to the voxels lying in between the pathology slides to assign each of these with a probability of their being malignant.

Patient selection

This cohort was derived from patients included in a separate multicentre study [11], in which patients were prospectively enrolled. All patients scheduled for radical prostatectomy at participating centres due to biopsy-proven prostate cancer were eligible for inclusion. For the current study, we selected a subset of patients who exhibited clearly distinguishable landmarks in both the pathology and ultrasound scan domains, which were necessary for assessing registration accuracy. The validity of these landmarks was determined by consensus between two independent observers (AJ and AP).

Registration accuracy

In order to calculate the target-registration error (TRE), the registration was performed with deliberate exclusion of the landmark as an input to the optimization algorithm, thereby mitigating its potential influence on the registration outcome. The landmarks could then be used to calculate the TRE between pathology and ultrasound.

Following registration, each landmark annotation on the pathology slides results in a group of registered landmark voxels in the ultrasound scan domain, of which the outer points were extracted. Subsequently, an ICP algorithm, similar to the one used in the registration process, was employed to obtain a translation that minimises the difference between the transformed outer voxel points and points on the landmark contour(s) obtained from the scan. To establish point pairs, the untransformed outer voxel point was paired with the point on the landmark contour lying closest to the translated outer voxel point. The TRE was then defined as the mean of the Euclidean distances between these point pairs. The magnitude of the TRE in the apex-base (AB), left-right (LR) and posterior-anterior (PA) axes only was also evaluated by projecting the distances onto each axis.

The TRE was determined for each patient, and the overall registration accuracy was subsequently expressed as the mean of these TREs.

Results

The total cohort consisted of 126 eligible patients, 20 of whom exhibited a clearly discernible landmark and were included in the registration accuracy analysis. The median prostate volume was 46.7mL (range 28.62–133.06). The identifiable landmarks on both imaging and pathology were predominantly cysts ($n = 9$) and calcifications ($n = 9$), with two additional cases of a clearly visible benign prostate hyperplasia (BPH) nodule observed on both ultrasound and pathology. A visualization of all ultrasounds, pathology slides, and registrations, including their corresponding landmarks, is provided in Supplementary Materials 1.

The overall registration accuracy, measured as the mean Target Registration Error (TRE), was 3.5 mm (range: 0.4–5.4 mm), with directional TRE values of 2.5 mm (apex-base), 1.1 mm (left-right), and 1.4 mm (posterior-anterior). Table 1 provides an overview of the per-patient TRE values and the types of landmarks identified. To evaluate potential confounding factors for TRE, a multivariate regression analysis was performed, incorporating prostate volume and landmark type. The analysis revealed a slight positive correlation between prostate volume and TRE, suggesting a trend toward higher TRE in larger prostates. However, this association was not statistically significant ($p = 0.179$). Likewise, calcifications as landmarks showed a non-significant increase in TRE ($p = 0.560$).

Discussion

Current guidelines recommend prostate MRI for men suspected of having PCa. While MRI has undoubtedly improved the diagnostic pathway for PCa, it is not without limitations, including variable diagnostic accuracy, interobserver variability, high cost, and limited availability [2, 3]. With population-based prostate cancer screening on the horizon, it is important to address potential challenges. The European Association of Urology (EAU) proposes a risk-adapted early detection strategy involving PSA testing for men aged 50 and older. If PSA levels exceed 3 ng/mL, further risk stratification using patient characteristics and a risk calculator is followed by prostate MRI if needed. A recent randomized study demonstrated MRI's selective power, as biopsies were avoided in 64.5% of men with negative MRIs (PI-RADS ≤ 2). However, among those with positive MRIs (PI-RADS ≥ 3), only 39% had clinically significant cancer, underscoring MRI's limitations regarding specificity [21].

The success of MRI in this context depends on its high negative predictive value (NPV) to avoid missing high-risk cancers. While high NPVs have been reported in specialized centres, general practice shows variability in MRI quality and radiologist expertise, potentially affecting screening outcomes across different regions and centers in a population-based program [22].

Multiparametric 3D TRUS offers a promising alternative, being relatively cost-effective, widely accessible,

Table 1 Per patient TRE

	Prostate volume (mL)	Landmark	TRE	TRE (AB)	TRE (LR)	TRE (PA)
1	133.06	Cyst	5.2	4.2	1.0	2.1
2	28.39	Calcification	1.9	1.5	0.2	0.1
3	33.46	Calcification	4.2	3.1	1.3	2.2
4	59.08	BPH nodule	2.5	1.3	0.8	1.8
5	88.54	Calcification	5.4	4.4	0.5	2.4
6	35.72	Calcification	5.3	3.6	2.9	2.0
7	80.15	Cyst	2.8	2.2	0.9	0.4
8	45.93	Calcification	3.8	2.6	1.4	2.0
9	45.97	Cyst	0.4	0.1	0.0	0.3
10	90.11	Cyst	4.3	2.5	1.6	3.0
11	76.87	Cyst	2.3	0.6	2.1	0.3
12	28.36	Cyst	3.1	2.6	0.7	0.8
13	62.10	Calcification	1.6	0.5	1.4	0.3
14	100.10	BPH Nodule	4.6	3.4	0.4	3.2
15	47.43	Calcification	4.3	3.5	0.6	1.1
16	28.75	Calcification	1.7	1.2	0.9	0.9
17	25.35	Cyst	5.1	3.8	2.0	3.4
18	47.70	Cyst	3.9	3.5	0.7	0.1
19	28.62	Calcification	4.9	3.9	1.5	1.4
20	27.29	Cyst	2.4	1.0	1.9	0.9
Mean	57.92	-	3.5	2.5	1.1	1.4
Median	46.7		3.9	2.6	0.9	1.3

TRE = target registration error, AB = pex-base, LR = left-right, PA = posterior-anterior, BPH = benign prostatic hyperplasia

and, when combined with AI, mitigating issues related to interobserver variability [11]. A fully AI-integrated workflow could enable automated cancer detection on TRUS imaging, serving as a computer-aided diagnostic tool in early detection programs to identify patients for prostate biopsy. Given that TRUS is also the imaging modality used for needle guidance during biopsy, this integration would facilitate direct targeting of suspicious lesions, reducing the targeting errors commonly associated with MRI-targeted biopsy. Furthermore, AI-driven segmentation and registration algorithms could enhance the accuracy and reproducibility of TRUS-pathology correlation, reducing interobserver variability. Machine learning models trained on large-scale datasets could also improve lesion characterization, potentially distinguishing between clinically significant and insignificant prostate cancer. These advancements could make TRUS a more viable and accessible alternative to MRI, particularly in settings with limited imaging resources. In a screening setting, multiparametric 3D ultrasound could serve as a replacement for MRI, especially in regions with limited MRI accessibility, or as a complementary modality. It could be used to pre-select patients for MRI, thereby reducing the overall MRI burden, or be performed alongside MRI to enhance diagnostic selectivity and accuracy.

However, developing a reliable AI-assisted ultrasound-based diagnostic tool for PCa diagnostics requires the creation of an accurate ground truth, which relies on precise registration between TRUS imaging and pathology.

The registration of RPS pathology to prostate imaging poses a considerable challenge, particularly in the context of TRUS. The current study presents a comprehensive framework for accurate registration of RPS to 3D TRUS, with a mean TRE of 3.5 mm based on 20 patients with clearly discernable landmarks. While there is no consensus on the maximum acceptable registration error, clinically significant PCa lesions are generally considered to have a volume of ≥ 0.5 cm^3, which corresponds to a diameter of 10 mm, assuming to lesion is spherical [16]. Therefore, we should aim to have a registration error below 10 mm.

This study makes significant advancements compared to existing literature in several areas.

Prior research has demonstrated the feasibility of registering pathology to ultrasound with acceptable levels of accuracy [18]. Our study builds upon this foundation by employing a larger dataset and a more comprehensive methodology. Notably, our study represents the first use of 3D acquired TRUS imaging, as opposed to relying on a 3D reconstruction from handheld 2D transversal sweeps. To ensure precise 3D RPS reconstruction, we implemented needle placement prior to RPS fixation, effectively preventing transitional and rotational errors. Furthermore, to aid the registration, we included compensation for the probe deformation. Although several assumptions and simplifications had to be made to model the deformation, it has shown to be a valuable addition to the registration process. Furthermore, while the use of anatomical structures for improving registration accuracy has generally been limited to the prostate border and urethra [15, 16, 18]. Based on our experience the addition of the border between PZ and TZ is feasible for most patients and is highly useful during registration. Although the visibility of ejaculatory ducts can vary (7 out of 20 cases in our dataset), when available, they offer valuable information during registration. When using ultrasound as the imaging modality, it is important to note that these ducts are generally only visible on CEUS and not on conventional B-mode. Additionally, landmarks had to be excluded from the registration to be able to calculate accuracy, but when included, they can provide information on slice and base thickness, and thus have a potential to improve accuracy. In our set of 20 patients, we had 3 patients with 2 landmarks available. For these patients, we repeated the registration but this time including the landmark that had not been used for validation. The new results and their differences compared to the old results are shown in Table 2.

Table 2 This table illustrates the effect of landmarks on the TRE. The values within the parentheses indicate change in TRE resulting from the integration of a landmark into the registration procedure

	TRE	TRE (AB)	TRE (LR)	TRE (PA)
1	4.9 (-0.6)	3.6 (-0.8)	0.6 (+0.1)	2.6 (+0.2)
2	2.7 (-1.2)	2.3 (-1.2)	0.6 (-0.1)	0.4 (+0.2)
3	2.3 (-2.3)	0.9 (-2.5)	0.7 (+0.3)	1.2 (-2.0)

TRE = target registration error, AB = apex-base, LR = left-right, PA = posterior-anterior, BPH = benign prostatic hyperplasia

This is a very small set of patients and therefore caution should be taken with any conclusions. However, all patients showed a significant overall improvement by inclusion of a landmark in the registration, especially in the apex-base direction.

Lastly, our study demonstrates the feasibility of including parasagittally cut apical slides in the pathology reconstruction, which has not been previously described due to the complexities involved in reconstruction [16]. These slides offer valuable information, as they often contain PCa lesions [23]. In fact, in our dataset, 75% of patients (15 out of 20) exhibited some form of prostate cancer in the apical pathology slides, underscoring the importance of including these slides in a ground truth dataset.

To optimize registration accuracy, several actions were taken during the handling of prostate specimens. A commercially available cutting device was employed to ensure uniform thickness of pathology slices, and needle

placement prior to fixation facilitated proper stacking of the slides after slicing.

The biggest uncertainty in the registration is in the apex-base axis, as we have the least information in that direction. To add further complexity, since the length of the prostate from apex to base may not be evenly divisible by 4, and the prostate is cut from apex to base, the thickness of the most basal slide often differs from the other slices. Although the inclusion of the apical slides aids in appropriately positioning the whole-mount slices from apex to base towards the apex, the most basal slides (i.e., bladder neck) were not included in the reconstruction process. The decision to exclude these slides stems from several factors. Firstly, the basal slice is typically larger than the apical slice and is cut thicker to facilitate the evaluation of extracapsular extension. Consequently, pathology slides originating from the basal slice are numerous and often need to be further divided to fit into pathology cassettes.

Moreover, the identification of the prostate border becomes more challenging in the vicinity of the urethra and seminal vesicles, further complicating the reconstruction of the basal slide. Additionally, it is worth mentioning that the incidence of prostate cancer in the base is generally low, further justifying the exclusion of the basal slide from the reconstruction process [24].

[25]. However, this leaves a significant range of possible values for the slice and base thicknesses, with the final chosen value dependent on the operator. This is reflected in our TRE calculations, which show that the TRE in the apex-base direction is twice as large as in the left-right and posterior-anterior directions.

Several limitations should be acknowledged in this study. Firstly, the small sample size limits the generalizability of the findings; future studies with larger cohorts are essential to validate the robustness and broader applicability of the proposed framework. Secondly, the manual segmentation, annotation and registration involved are time intensive, costing approximately an hour per prostate. Efforts to automate segmentation of ultrasound images through deep learning algorithms have shown promising results and are expected to reduce the required manual labor. Moreover, the manual nature of these procedures introduces the possibility of interobserver variability. Certain ultrasound segmentations, such as those for the urethra and zones, may not always be clearly visible, particularly in cases involving larger prostates. Although consensus meetings were held among operators to address uncertainties in specific segmentations, it is important to acknowledge that this process may have influenced the registration accuracy to some extent. A suggested improvement to the registration algorithm would be to provide it with a weighting factor for each segmentation point based on the quality of the scan at that location. This would allow the registration to put more focus on more clearly visible– and therefore more certain - areas of the US segmentations. Another possible limitation is the handling of incomplete pathology sections during reconstruction that arise from tissue damage and other artefacts on the pathology slides. While large missing sections or smaller gaps adjacent to PCa regions were addressed by requesting new pathology slides, smaller missing areas not adjacent to PCa were assumed to be negative for malignancy. This assumption introduces a potential source of error, as it may overlook rare cases where cancerous tissue could be present in these areas.

Lastly, the registration method employed in this study requires custom-made software for execution, which may present challenges when implementing it elsewhere. However, the authors can be contacted for assistance in research projects, and they are willing to share data upon reasonable request, facilitating further exploration and collaboration in the field.

Conclusion

The study presents a comprehensive framework for registering RPS pathology to 3D TRUS, achieving accurate results based on discernable landmarks. Precise registration is crucial for generating reliable datasets, essential in developing and validating new diagnostic tools and for training AI-assisted imaging modalities.

Supplementary Information

The online version contains supplementary material available at https://doi.org/10.1186/s12894-025-01736-4.

Supplementary materials 1: A visualization the ground truth for all 20 included patients. The 3D segmentations the ultrasound scans are visualized in red and green, red being the right prostate lobe and green the left. Within the prostate in yellow the border between the TZ and PZ is visualized, as well as the urethra and the spermatic ducts. The pathology slides are mapped onto the segmented ultrasound scans, the borders of which are shown as purple dots and blue lines

Acknowledgements

Acknowledgements: Anna Garrido Utrilla.

Author contributions

AJ: Conceptualization, Methodology, Acquisition, Writing– Original Draft, Visualization, Project administration. MZ: conceptualization, Methodology, Writing– Original Draft, Visualization, Project administration, interpretation of data, statistical analysis. DK & AP: Conceptualization, Methodology, Acquisition, Writing– Review & Editing. WZ: Methodology, interpretation of data, statistical analysis. JO: Writing– Review & Editing, Supervision, Funding acquisition. HB: Writing– Review & Editing, Supervision, Funding acquisition. MM: Conceptualization, Methodology, Writing– Review & Editing, Supervision, Project administration. All authors read and approved the final paper.

Funding

This work was supported by the European Union and Angiogenesis Analytics.

Data availability
The datasets used and/or analyzed during the current study are available from the corresponding author on reasonable request.

Declarations

Conflict of interest
HB is chair of the clinical board for AA. AP and MM are scientific advisors for AA for which they receive compensation. MZ and WZ are employees of AA.

Ethics approval and consent to participate
this study was approved by an accredited medical research ethics committee (MEC AMC) under reference number 2020_268#B202178. All study participants signed an informed consent form that includes the consent for use of their data for publication. The study was performed in accordance with the Declaration of Helsinki.

Clinical trial number
NCT04605276.

Received: 7 October 2024 / Accepted: 5 March 2025
Published online: 03 April 2025

References

1. Mottet N, van den Bergh RCN, Briers E, Van den Broeck T, Cumberbatch MG, De Santis M, et al. EAU-EANM-ESTRO-ESUR-SIOG guidelines on prostate Cancer-2020 update. Part 1: screening, diagnosis, and local treatment with curative intent. Eur Urol. 2021;79(2):243–62.
2. Drost FH, Osses D, Nieboer D, Bangma CH, Steyerberg EW, Roobol MJ, Schoots IG. Prostate magnetic resonance imaging, with or without magnetic resonance Imaging-targeted biopsy, and systematic biopsy for detecting prostate cancer: A Cochrane systematic review and Meta-analysis. Eur Urol. 2020;77(1):78–94.
3. Brembilla G, Dell'Oglio P, Stabile A, Damascelli A, Brunetti L, Ravelli S, et al. Interreader variability in prostate MRI reporting using prostate imaging reporting and data system version 2.1. Eur Radiol. 2020;30(6):3383–92.
4. Lisney AR, Leitsmann C, Strauss A, Meller B, Bucerius JA, Sahlmann CO. The role of PSMA PET/CT in the primary diagnosis and Follow-Up of prostate Cancer-A practical clinical review. Cancers (Basel). 2022;14(15).
5. Mannaerts CK, Engelbrecht MRW, Postema AW, van Kollenburg RAA, Hoeks CMA, Savci-Heijink CD, et al. Detection of clinically significant prostate cancer in biopsy-naive men: direct comparison of systematic biopsy, multiparametric MRI- and contrast-ultrasound-dispersion imaging-targeted biopsy. BJU Int. 2020;126(4):481–93.
6. Turkbey B, Haider MA. Deep learning-based artificial intelligence applications in prostate MRI: brief summary. Br J Radiol. 2022;95(1131):20210563.
7. de Rooij M, van Poppel H, Barentsz JO. Risk stratification and artificial intelligence in early magnetic resonance Imaging-based detection of prostate Cancer. Eur Urol Focus. 2021.
8. Wildeboer RR, Mannaerts CK, van Sloun RJG, Budaus L, Tilki D, Wijkstra H, et al. Automated multiparametric localization of prostate cancer based on B-mode, shear-wave elastography, and contrast-enhanced ultrasound radiomics. Eur Radiol. 2020;30(2):806–15.
9. Yi Z, Hu S, Lin X, Zou Q, Zou M, Zhang Z, et al. Machine learning-based prediction of invisible intraprostatic prostate cancer lesions on (68) Ga-PSMA-11 PET/CT in patients with primary prostate cancer. Eur J Nucl Med Mol Imaging. 2022;49(5):1523–34.
10. Suarez-Ibarrola R, Sigle A, Eklund M, Eberli D, Miernik A, Benndorf M et al. Artificial intelligence in magnetic resonance Imaging-based prostate Cancer diagnosis: where do we stand in 2021? Eur Urol Focus. 2021.
11. Jager A, Postema AW, Mischi M, Wijkstra H, Beerlage HP, Oddens JR. Clinical trial protocol: developing an image classification algorithm for prostate Cancer diagnosis on Three-dimensional multiparametric transrectal ultrasound. Eur Urol Open Sci. 2023;49:32–43.
12. Wildeboer RR, van Sloun RJG, Huang P, Wijkstra H, Mischi M. 3-D Multi-parametric Contrast-Enhanced ultrasound for the prediction of prostate Cancer. Ultrasound Med Biol. 2019;45(10):2713–24.
13. Wildeboer RR, Van Sloun RJG, Schalk SG, Mannaerts CK, Van Der Linden JC, Huang P, et al. Convective-Dispersion modeling in 3D Contrast-Ultrasound imaging for the localization of prostate Cancer. IEEE Trans Med Imaging. 2018;37(12):2593–602.
14. Willemink MJ, Koszek WA, Hardell C, Wu J, Fleischmann D, Harvey H, et al. Preparing Med Imaging Data Mach Learn Radiol. 2020;295(1):4–15.
15. Rusu M, Shao W, Kunder CA, Wang JB, Soerensen SJC, Teslovich NC, et al. Registration of presurgical MRI and histopathology images from radical prostatectomy via RAPSODI. Med Phys. 2020;47(9):4177–88.
16. Wildeboer RR, van Sloun RJG, Postema AW, Mannaerts CK, Gayet M, Beerlage HP, et al. Accurate validation of ultrasound imaging of prostate cancer: a review of challenges in registration of imaging and histopathology. J Ultrasound. 2018;21(3):197–207.
17. Shao W, Banh L, Kunder CA, Fan RE, Soerensen SJC, Wang JB, et al. ProsRegNet: A deep learning framework for registration of MRI and histopathology images of the prostate. Med Image Anal. 2021;68:101919.
18. Schalk SG, Postema A, Saidov TA, Demi L, Smeenge M, de la Rosette JJ, et al. 3D surface-based registration of ultrasound and histology in prostate cancer imaging. Comput Med Imaging Graph. 2016;47:29–39.
19. Jager A, Postema AW, van der Linden H, Nooijen P, Bekers E, Kweldam CF, et al. Reliability of whole Mount radical prostatectomy histopathology as the ground truth for artificial intelligence assisted prostate imaging. Virchows Arch. 2023;483(2):197–206.
20. Jonmarker S, Valdman A, Lindberg A, Hellstrom M, Egevad L. Tissue shrinkage after fixation with formalin injection of prostatectomy specimens. Virchows Arch. 2006;449(3):297–301.
21. Hugosson J, Mansson M, Wallstrom J, Axcrona U, Carlsson SV, Egevad L, et al. Prostate Cancer screening with PSA and MRI followed by targeted biopsy only. N Engl J Med. 2022;387(23):2126–37.
22. Sathianathen NJ, Omer A, Harriss E, Davies L, Kasivisvanathan V, Punwani S, et al. Negative predictive value of multiparametric magnetic resonance imaging in the detection of clinically significant prostate Cancer in the prostate imaging reporting and data system era: A systematic review and Meta-analysis. Eur Urol. 2020;78(3):402–14.
23. Veerman H, Boellaard TN, van Leeuwen PJ, Vis AN, Bekers E, Hoeks C, et al. The detection rate of apical tumour involvement on preoperative MRI and its impact on clinical outcomes in patients with localized prostate cancer. J Robot Surg. 2022;16(5):1047–56.
24. Vargas SO, Jiroutek M, D'Amico AV, Renshaw AA. Distribution of carcinoma in radical prostatectomy specimens in the era of serum prostate-specific antigen testing. Implications for delivery of localized therapy. Am J Clin Pathol. 1999;112(3):373–6.
25. Sakamoto Y, Fukaya K, Haraoka M, Kitamura K, Toyonaga Y, Tanaka M, Horie S. Analysis of prostate cancer localization toward improved diagnostic accuracy of transperineal prostate biopsy. Prostate Int. 2014;2(3):114–20.

Publisher's note